Journal of Advanced Research 83 (2026) 379–390

Contents lists available at ScienceDirect

Journal of Advanced Research

journal homepage: www.elsevier.com/locate/jare

Original Manuscript

Longitudinal prediction of drug response in high-grade serous ovarian cancer organoid cultures aligning with clinical responses

Enrico Cavarzerani [a], Isabella Caligiuri [b], Michele Bartoletti [c], Giuseppe Corona [d], Tiziana Perin [b], Antonio Palumbo [b], Antonino Ditto [e], Tommaso Occhiali [e], Vincenzo Canzonieri [b,f,*], Flavio Rizzolio [a,b,**]

[a] Department of Molecular Sciences and Nanosystems, Ca' Foscari University of Venice, 30172 Venezia, Italy
[b] Pathology Unit, Centro di Riferimento Oncologico di Aviano (CRO) IRCCS, 33081 Aviano, Italy
[c] Unit of Medical Oncology and Cancer Prevention, Department of Medical Oncology, Centro di Riferimento Oncologico di Aviano (CRO), IRCCS, 33081 Aviano, Italy
[d] Immunopathology and Cancer Biomarkers, CRO Aviano, National Cancer Institute, IRCCS, 33081 Aviano, Italy
[e] Gynecologic Oncology Unit, Centro di Riferimento Oncologico, National Cancer Institute, Aviano, Italy
[f] Department of Medical, Surgical and Health Sciences, University of Trieste 34127 Trieste, Italy

HIGHLIGHTS

- PDTOs from ovarian cancer can reliably predict drug response after extensive passaging.
- PDTO sensitivity to 19 FDA drugs correlates with clinical outcomes.
- The platform enables direct comparison of experimental and clinical drugs for personalized use.
- The study confirms platform's stability, validating a biobank concept for consistent responses.
- PDTOs resistant to first-line therapy could be instrumental in identifying potent novel experimental drugs (Pin1 inhibitors).

GRAPHICAL ABSTRACT

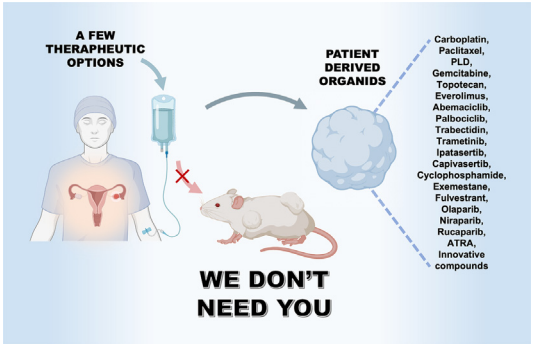

ARTICLE INFO

Article history:
Received 18 October 2024
Revised 1 May 2025
Accepted 6 August 2025
Available online 7 August 2025

Keywords:
High-grade serous ovarian cancer
Patient-derived organoids
Drug screening
Personalized therapy
Peptidylprolyl Cis/Trans Isomeras NIMA-Interacting 1 (Pin1)

ABSTRACT

Introduction: High-grade serous ovarian cancer (HGSOC) ranks among the most aggressive gynecological malignancies. Its high mortality is driven by frequent recurrence after primary treatments and the development of platinum resistance. Traditional drug development using animal models is time-consuming and often lacks reproducibility, making it less effective for precision cancer medicine.
Objectives: This study aimed to demonstrate the potential of primary patient-derived tumor organoids (PDTOs) as a platform to replicate disease pathophysiology and accelerate drug screening for HGSOC. The focus was on validating the stability of PDTOs in predicting drug responses over time and comparing *in vitro* results with clinical data.
Methods: An expandable HGSOC PDTO platform was developed for rapid drug screening and resistance testing. Seven pairs of organoids underwent low- and high-passage drug screenings over up to a nine-month period. The screenings involved 20 conventional and FDA-approved drugs, and proteomic analyses were conducted to assess the stability of the organoids over time.
Results: The comparison of *in vitro* drug screening outcomes with clinical data confirmed the predictive capacity of the organoid platform. Notably, a PDTO with a BRCA1 mutation exhibited resistance to

* Corresponding author at: Pathology Unit, Centro di Riferimento Oncologico di Aviano (CRO) IRCCS, 33081 Aviano, Italy.
** Corresponding author at: Department of Molecular Sciences and Nanosystems, Ca' Foscari University of Venice, 30172 Venezia, Italy.
E-mail addresses: vcanzonieri@cro.it (V. Canzonieri), flavio.rizzolio@unive.it (F. Rizzolio).

https://doi.org/10.1016/j.jare.2025.08.009

Carboplatin and PARP inhibitors, reflecting the clinical scenario and reinforcing the platform's predictive power.

Conclusion: This study underscores the clinical significance of organoid models in predicting drug resistance and therapeutic response. These models demonstrated their utility in screening novel treatments, such as Peptidylprolyl Cis/Trans Isomerase, NIMA-Interacting 1 (Pin1) inhibitors, which show potential in overcoming resistance to standard ovarian cancer therapies. The organoid platform offers a powerful tool for advancing personalized treatment approaches, with the capability to guide therapeutic decisions and optimize patient outcomes.

Introduction

Lethal diseases require more biologically relevant models to advance the development of accurate diagnostic and therapeutic strategies. Among preclinical models, mouse models have been the most extensively used and remain widely adopted due to several advantages, including rapid reproduction, relatively low cost, genetic stability, and a well-established body of scientific literature [1–3]. These attributes have enabled the discovery of fundamental biological mechanisms underlying both Mendelian and complex diseases, including cancer.

HGSOC is one of the most lethal gynecological malignancies and has garnered increasing attention in recent years due to significant advances in the identification of its tissue of origin, as well as the establishment of novel cell lines and animal models [4–7]. In parallel, comprehensive genomic analyses have revealed actionable mutations and molecular alterations that hold promise for targeted therapeutic strategies. However, despite these advancements, overall survival rates for HGSOC patients remain dismally low [4,8–11]. As a result, there is a continued effort within the scientific community to develop and refine alternative preclinical models with the goal of improving our understanding of HGSOC biology and enhancing clinical outcomes [5,12,13]. Among *in vitro* models, organoid technology has emerged as a promising and innovative approach [14]. Pioneering studies have demonstrated that adult stem cells can give rise to crypt–villus structures containing all differentiated intestinal cell types, while embryonic stem cells are capable of forming self-organizing structures that recapitulate key spatial and temporal features of early neuronal development [15,16].

Subsequently, organoid technology has been successfully applied to model a wide range of tissues and organs, including HGSOC [17,18]. Single epithelial cells isolated from the fallopian tube have been shown to generate organoid cultures when embedded in a three-dimensional extracellular matrix and supplemented with Wnt, Notch, EGF, FGF10, and TGF-β signaling factors. These cells retain the ability to proliferate and differentiate into secretory and ciliated cell lineages [19]. Genetically engineered organoids derived from both fallopian tube and ovarian surface epithelium in mouse models have been used to recapitulate HGSOC, although they exhibit distinct phenotypic characteristics, tumor latency, and molecular signatures, which correlate with differential responses to chemotherapy [12]. Furthermore, organoids generated from immunocompetent mice harboring specific genetic alterations demonstrated genotype-dependent differences in chemosensitivity, secretome profiles, and immune microenvironment composition. This platform enabled the identification of an effective combination therapy for the CCNE1-amplified HGSOC subtype [20].

In 2018, Hill Sarah et al. established thirty-three short-term cultures of HGSOC human organoids to identify targetable DNA damage repair defects [17]. Functional defects in the homologous recombination (HR) pathway have been shown to correlate with sensitivity to poly (ADP-ribose) polymerase (PARP) inhibitors, while deficiencies in replication fork protection have been associated with sensitivity to carboplatin, CHK1 inhibitors, and ATR inhibitors [17]. The HR pathway plays a crucial role in repairing DNA double-strand breaks, and its dysfunction can lead to genomic instability and tumorigenesis. PARP inhibitors exploit the concept of synthetic lethality in cancer cells with HR deficiencies, leading to cell death [21]. In contrast, replication fork protection mechanisms are essential for maintaining genome stability during DNA replication, and their impairment can sensitize cells to DNA-damaging agents, such as carboplatin, CHK1 inhibitors, and ATR inhibitors [17,21,22]. The ability of organoids to predict drug sensitivity was confirmed and expanded demonstrating that it is possible to derive long-term cultures of ovarian cancer (OC) organoids representing all main subtypes. Intra- and interpatient heterogeneity was detected, as well as the acquisition of chemoresistance in recurrent disease [23]. These data were confirmed by other groups demonstrating the potential use of organoids for clinical decision-making [24–26]. Our group also demonstrated that HGSOC organoids can be used to test drugs currently on the market or novel drugs [27–38]. While some published papers have supported the utilization of PDTOs as a promising predictive biomarker in cancer treatment, [39], only a few studies have demonstrated the ability of organoids to predict drug response after long-term culture. For instance, colorectal cancer organoids were tested with 11 different drugs at the beginning and after 1 month of culture, showing good to fair reproducibility [40]. While some studies demonstrate reproducibility and retention of patient-specific characteristics in OC organoids over long-term cultures [23,24,41,42], none have directly assessed changes in drug response. This highlights a significant gap in current research, emphasizing the need for further exploration into the stability of drug responsiveness in organoid cultures over extended periods. Moreover, we explored the potential to develop novel targeted therapies and testing new inhibitor of Pin1, an emerging target of HGSOC as demonstrating by our group [27,33,43,44].

Material and methods

Organoid cultures

Organoids were derived from completely de-identified specimens; however, written informed consent for research purposes was obtained to collect the samples at the Pathology Unit of the National Cancer Institute (CRO) of Aviano (approval no. 17197). For ascitic fluids, cells in the pellets were isolated by centrifugation at 1000 rpm for 10 min and subsequently washed twice with Hank's Balanced Salt Solution (HBSS, Gibco, Massachusetts, United States). To remove erythrocytes from the fluid, cold red blood cell lysis buffer (Roche Diagnostics, Basel, Switzerland) was added and incubated on ice with continuous stirring for 10 min. The cell pellet was centrifuged at 1,000 rpm for 10 min and resuspended in Cultrex RGF BME, Type 2 (Bio-techne, Minnesota, USA). Solid tumor

tissues were incubated in Dulbecco's Modified Eagle's Medium/Nutrient Mixture F-12 Ham without Phenol red supplemented with Levofloxacin (100 μg/mL), Vancotex (25 μg/mL), Ciproxin (5 μg/mL), Gentamicin (200 μg/mL), and Fungizone (5 μg/mL) for 30 min. The tissues were then finely minced into pieces of approximately 0.5–1 mm diameter using fine dissection scissors. A solution of 4 mg/mL collagenase IV (Gibco, Massachusetts, United States) was added to the minced tissues, which were incubated at 37 °C for no more than 45 min and mechanically dissociated by pipetting. The cell clusters were pelleted by centrifugation at 1,000 rpm for 10 min, resuspended in an appropriate volume of Cultrex RGF BME, Type 2 (Bio-techne, Minnesota, United States), and then seeded in 24-well cell culture plates. Following the polymerization of Cultrex, 500 μL of organoid culture medium, as described by Kopper et al., was added to each well and replenished every 3 days [23]. The organoids were cultured at 37 °C in a 5 % CO2 environment.

Immunohistochemistry

Sections of formalin-fixed, paraffin-embedded ascites and solid tumor PDOs were used for histopathological analyses. Upon reaching passage 2, PDTOs were recovered from BME using ice-cold cell recovery solution (Corning, New York, United States) in accordance with manufacturing protocols, fixed in phosphate-buffered 10 % formalin, and embedded in 500 μL of Bio-Agar (Bio-Optica Milano Spa, Milano, ITA). Five μm sections were stained with hematoxylin and eosin (H&E) using a Leica ST5020 multistainer and 2 μm sections were cut for immunohistochemistry (IHC) analysis. The IHC was performed with an UltraVision LP Detection System HRP DAB kit (Thermo Scientific, Waltham, USA). Heat-induced antigen retrieval was performed using 10 mM citrate buffer pH 6.0. The following antibodies were used to characterize PDTOs and parental tumors: PAX8 (ProteinTech Group, Germany, EU), WT1 (Abcam, U.K.), CA-125 (Santa Cruz Biotechnology, TX), TP53 (ProteinTech Group, Germany, EU) and Pin1 (Santa Cruz Biotechnology, California, USA).

Viability assays

Clusters of organoids were homogenized in an appropriate volume of Cultrex RGF BME, Type 2, and 2 μL of this homogenate and seeded in 96-well plates. Viability assessments were conducted using the PrestoBlue HS Assay (Thermo Fisher Scientific Inc, Massachussets, USA) at 2, 4, 7, and 9-day intervals, following manufacturer's protocols. Viability measurements were performed in four replicates, and p-values were calculated using a two-tailed Student's *t*-test with GraphPad Prism (La Jolla, CA, United States). The p-values were denoted as follows: * $p \leq 0.05$, ** $p \leq 0.01$, *** $p \leq 0.001$, and **** $p \leq 0.0001$.

Half-maximal inhibitory concentration (IC50) and deciphering drug effectiveness

Clusters of organoids were mixed in an appropriate volume of Cultrex RGF BME, Type 2, and 2 μL of this mixture were seeded in 96-well plates in five replicates for low and high passage organoids both. After 24 h, organoids were exposed to six 1:5 serial dilutions of drugs starting from 200 μM (Carboplatin, Paclitaxel, Gemcitabine, Everolimus, Abemaciclib, Trametinib, Ipatasertib, Capivasertib, ATRA, VS10), 100 μM (PLD, Topotecan, Palbociclib, Cyclophosphamide, Exemestane, Fulvestrant, Olaparib, Niraparib, Rucaparib), or 10 μM (Trabectedin). After 96 h, cell viability was measured using CellTiter-Glo 3D (Promega, Madison, WI, United States). The luminescence was acquired with BioTek Synergy H1. Logistical dose–response curves were used to calculate IC50 and AUC using GraphPad Prism (La Jolla, CA, US).

The interpretation of the IC50 values for the construction of the heatmap was done on the basis of the algorithm proposed by Brook et al. [45]. The initial qualitative assessment of the drug response curve is essential to ascertain whether the calculation of the IC50 value is viable, thereby discriminating drugs for which the patient is sensitive from those that are not (shown in the heatmap of Fig. 5 in grey).

The IC50 values for drug-sensitive PDTOs were calculated and organized according to their increasing magnitude; a color gradient from red (indicating the lowest IC50 value) to blue (200 μM) was assigned. The method used for this interpretation process is exemplified in Fig. S1.

Proteomic analysis

The PDTOs (approximately 400,000 cells) were isolated and collected using Cell Recovery Solution (Corning, New York, USA) to eliminate the Basement Membrane Extract (BME). They were subsequently subjected to three washes with Hank's Balanced Salt Solution (HBSS). Peptide extraction was performed using the Easy-Pep™ MS Sample Prep Kits (Thermo Fisher Scientific Inc, Massachusetts, USA), following the manufacturer's protocol. Subsequently, the samples were lyophilized, and then reconstituted in 0.1 % Formic Acid in MilliQ water. Two mg of desalted digested peptides were loaded and fractionated on Peptide XBridge C18 150 x 2.1 mm column (Waters, Milford, MA, USA) maintained at 40 °C and flowed at 0.2 mL/min using Horizon Vanquish UPLC instrument (Thermos Scientific, San Jose, CA, USA). Mobile phase A consisted of water and 0.1 % formic acid while mobile phase B consisted of acetonitrile 0.1 % formic acid. Peptides are eluted from the column using the following gradient: mobile phase B increased from 1 % to 35 % over 30 min, followed by 90 % B in 5 min, and the column was washed for 1 min at 90 % B and then re-equilibrated for 10 min at 1 % B. The eluting peptides from the column were analyzed on a quadrupole-ion trap-Orbitrap QExactive Plus mass spectrometer (Thermo Scientific, San Jose, CA). Orbitrap survey MS1 scans from 375 m/z to 1500 m/z were performed at a resolving power of 70,000 at 200 m/z with an AGC target of $3x10^6$ ions and maximum injection time set to 100 ms. All tandem MS scans were performed on precursors with 2–8 charge states, using HCD fragmentation with normalized collision energy of 20 and dynamic exclusion of 30 s. The instrument was operated in the TNop10 mode and the MS/MS scan was performed at the resolving power of 35,000 using an ion count target set to 1×10^5 and the maximum injection time of 114 ms. Precursors were isolated using a quadrupole isolation window of 2.2 m/z. Proteome Discoverer 2.5 software (Thermo Scientific, San Jose, CA, USA) processed the raw acquisition file for protein ID and label-free quantification of organoid proteomics profile at early and late stages. The parameters used for ID and LFQ were mass tolerance of 10 ppm for MS1 and 0.02 Da for MS2. The target false discovery rate (FDR) was set to 1 % while MS/MS spectra were searched by Sequest against a reviewed *Homo sapiens* database (SwissProt, November 2023, 20,418 entries) using the following parameters: trypsin digestion, maximum of two missed cleavages, cysteine carbamidomethylation as fixed modification, methionine oxidization, protein N-terminal acetylation, and de-methylation as variable modifications. Label-free quantification was performed by exploiting unique and razor peptides for protein abundance calculation.

Genomic characterization of PDTO

Sample collection and DNA extraction

All patients underwent clinically relevant mutation analysis tailored to their specific diagnosis. For in depth analysis of patient 2, formalin-fixed, paraffin-embedded (FFPE) ovarian tumor tissue

specimens were obtained from patients diagnosed with epithelial ovarian carcinoma, in accordance with Ethical Committee approval and after obtaining written informed consent. Tissue blocks were sectioned at 5–10 μm thickness, and tumor-rich areas were macrodissected under histopathological guidance to ensure ≥70 % tumor cellularity. Genomic DNA was extracted using the QIAamp DNA FFPE Advanced UNG Kit (Qiagen, cat. no. 56704), which includes an enzymatic deparaffinization and uracil-DNA glycosylase (UDG) treatment step to reduce formalin-induced sequence artifacts. The protocol was followed as recommended by the manufacturer, with extended lysis time to optimize DNA recovery from highly crosslinked FFPE materials. Extracted DNA was eluted in low-EDTA TE buffer and quantified using a Qubit dsDNA HS Assay Kit (Thermo Fisher Scientific). DNA integrity was assessed with a TapeStation 4200 system (Agilent Technologies), and the DNA Integrity Number (DIN) was used as a metric for quality control. Only samples with DIN > 4 and DNA concentration ≥10 ng/μL were considered suitable for library preparation and downstream targeted sequencing.

Targeted DNA sequencing

Targeted sequencing was carried out using the QIAseq Targeted DNA Pro Human Colorectal Cancer Research Panel (Qiagen), which enables comprehensive profiling of 71 genes, including key oncogenes and tumor suppressor genes relevant across multiple solid tumor types. The panel also includes genes commonly altered in gynecologic malignancies, enabling cross-cancer pathway analysis and identification of potentially actionable variants: AKT1, APC, ARID1A, ATM, BARD1, BRAF, BRCA1, BRCA2, BRIP1, CDK12, CDKN2A, CHEK1, CHEK2, CTNNB1, EGFR, ERBB2, FGFR1, FGFR3, KRAS, MAP2K1, MET, MLH1, MSH2, MSH6, MUTYH, MYC, NRAS, PALB2, PIK3CA, PMS1, PMS2, POLD1, POLE, PTEN, RAD51B, RAD51D, RET, RNF43, SMAD4. Library preparation followed the QIAseq DNA Pro workflow, which integrates unique molecular indices (UMIs) to enhance error correction and improve the accuracy of low-frequency variant detection. Briefly, 40 ng of high-quality genomic DNA per sample was enzymatically fragmented, end-repaired, and ligated to adapters containing UMIs and sample-specific indices. Target enrichment was achieved via single-primer extension (SPE)–based multiplex PCR amplification. Final libraries were purified using AMPure XP beads (Beckman Coulter) and quantified by qPCR before pooling for sequencing.

Sequencing and data analysis

Pooled libraries were sequenced on an Illumina MiSeq platform using the MiSeq Reagent Kit v2 with a paired-end 2 × 150 bp configuration. For each sequencing run, a maximum of 10 ovarian tumor samples were multiplexed to ensure optimal read depth and coverage across all targeted regions. Demultiplexed FASTQ files were processed through the QIAGEN GeneGlobe Data Analysis Center, a cloud-based analysis platform specifically designed for QIAseq technologies. The QIAseq Targeted DNA Pro pipeline was employed for bioinformatic analysis, incorporating UMIs for robust error correction and accurate variant detection. Reads were aligned to the human reference genome (GRCh38) using a UMI-aware algorithm, which collapses PCR duplicates into consensus reads. Variant calling was performed using a proprietary algorithm optimized for the QIAseq panel design, followed by automatic filtering based on key quality metrics including read depth, strand bias, and base quality. Only high-confidence somatic variants with an allele frequency ≥5 % and a minimum coverage of 100× were retained. Annotated variant data were cross-referenced against multiple databases, including COSMIC, ClinVar, dbSNP, and gnomAD, to assess known pathogenicity, population frequency, and potential clinical relevance. Additional manual curation was conducted to identify recurrent mutations and potential overlaps with colorectal cancer–associated mutational landscapes.

Generation of resistant PDTOs

To evaluate the emergence of drug resistance under sustained therapeutic pressure, PDTOs derived from Patient 3 were subjected to a stepwise selection protocol using increasing concentrations of carboplatin. Organoids were cultured in high-density conditions within 96-well plates and exposed sequentially to three escalating doses of carboplatin: 50 μM, 75 μM, and 100 μM. Each drug concentration was applied for one week, with fresh medium and drug replenished every 24 h.

At the end of each treatment cycle, viable organoids were recovered by mechanical dissociation with Cell Recovery Solution (Corning, New York, USA), re-plated into fresh Cultrex RGF BME, and cultured for 48 h before initiating the next round of carboplatin exposure. Viability was assessed daily using the PrestoBlue™ HS Cell Viability Reagent (Thermo Fisher Scientific), and normalized as fold-change relative to baseline (t/t_0). Data were collected from five biological replicates for each condition.

For fluorescence images, organoids were stained at day 0, 5, 12, and 19 for 40 min with Calcein AM 0,50 μM, washed twice with HBSS, and stained with EthD-1 0,25 μM for 40 min. After being washed twice with HBSS, 100 μL DMEM/F12 without phenol red was applied and the fluorescence was observed in a EVOS FL AUTO 2 mycroscope (Thermo Fisher Scientific Inc, Massachusetts, USA).

Results and discussion

Establishment of a living biobank of OC patients

As depicted in Fig. 1A, B, tumor organoid cultures were obtained from seven different patients. All these PDTOs were effectively cultured from tumor specimens, resulting in PDTOs that are highly expandable and sustainable for long-term culturing. Two PDTOs were derived from the primary tissue and 5 from ascites. Of note, organoid formation efficiency did not significantly differ between ascites and primary tissues [46].

All patients were diagnosed and treated for FIGO stage IIIB-IV epithelial OC and main histological subtypes and molecular subgroups were well represented.

Patient 1 was diagnosed with low grade serous ovarian cancer (LGSOC) at age of 32. The clinical course showed an aggressive and platinum resistant behavior. Ascites were collected at the time of platinum-resistant recurrence. Molecular analysis performed on formalin fixed, paraffin embedded tumor tissue showed all-RAS-BAF wild type, BRCA 1–2 wild type, mismatch repair proficiency. Patient 2 was diagnosed with FIGO stage IIIC HGSOC and a pathogenic BRCA1 mutation was unveiled. After primary surgery and platinum chemotherapy, she received maintenance with olaparib for only 6-months before experiencing a recurrence of peritoneal disease. Ascites were collected at the time of recurrence. Patients 3, 4 and 7 with HGSOC were treated with cytoreductive surgery and platinum chemotherapy and have a BRCA 1–2 wild type status. Patient 5 was diagnosed with clear cell carcinoma and she died few months after the end of platinum-based chemotherapy. Patient 6 was diagnosed with HGSOC with a partial mucinous differentiation.

OC-derived organoids reproduce the original tumor phenotype

As depicted in Fig. 1B, variations in the growth rate of the PDTOs under investigation were observed. Notably, achieving passage 5 took one month for some PDTOs, while it required nine months

A

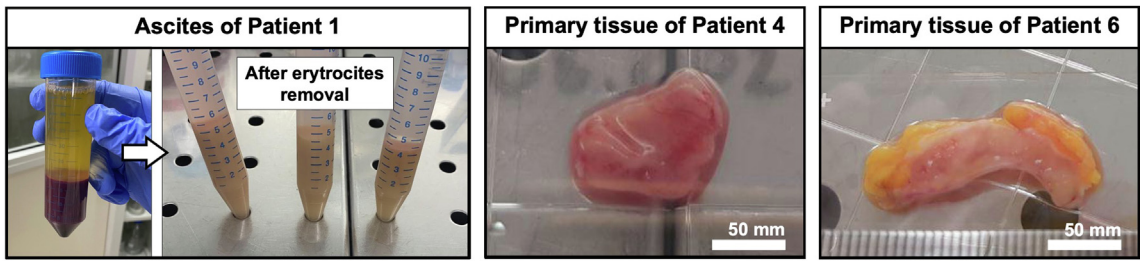

B

Sample	OC Type	FIGO stage at diagnosis	Recourrence	Patient status	Origin	PDTO Morphology	Passaging time
PDTO-Pat1	LGSOC	IVB	Yes	Death	Ascites	Cystic	Long-term (p5 in 2 months)
PDTO-Pat2	HGSOC	IIIC	Yes	Death	Ascites	Dense	Long-term (p5 in 3 months)
PDTO-Pat3	HGSOC	IIIC	Yes	Death	Ascites	Low-cohesive	Long-term (p5 in 9 months)
PDTO-Pat4	HGSOC	IIIC	NA	NA	Primary tissue	Low-cohesive	Long-term (p5 in 1 month)
PDTO-Pat5	CCC	IIIC	Yes	Death	Ascites	Dense	Long-term (p4 in 8 months)
PDTO-Pat6	HGSOC MC	IIIC	No	Alive	Primary tissue	Dense	Long-term (p5 in 2 months)
PDTO-Pat7	HGSOC	NA	NA	Death	Ascites	Dense	Long-term (p5 in 5 months)

Fig. 1. OC Patients, Establishment of Organoid Lines and biobanking: (A) An example of primary tumor and ascites samples derived from patients 1, 4 and 6, before processing for organoid culture. (B) Summary of the patient/organoid characteristics: HGSOC, high grade serous ovarian cancer; LGSOC, low grade serous ovarian cancer; CCC, clear cell carcinoma; MC, mucinous carcinoma; long-term cultures refer to organoids with a high passageability (higher than 5 passages).

for others, probably reflecting the heterogeneous composition of the tumors. In this respect, all the organoids have been characterized by H&E staining together with IHC of PAX8, WT1, CA125 and TP53 markers (Fig. 2), evaluated by two pathologists and summarized in Fig. 2C. PAX8 (paired box) gene is a transcription factor primarily associated with fallopian tube development and is not essential for ovarian development. In contrast to PAX8, PAX2 is typically downregulated early in the progression of serous OC. However, PAX8 maintains ubiquitous expression, underscoring its role in processes such as migration, invasion, proliferation, cell survival, stem cell maintenance, and tumor growth as analyzed in the study of Hardy et al. [47]. As a result, PAX8 is utilized as a marker for the detection of HGSOC, with PAX8 expression observed in both primary tumors and ascites, as well as in PDTOs [47]. The expression of Wilms' Tumor 1 (WT1) has been documented in various adult cancers [48,49]. Within the female genital tract, its localization is employed as a discriminative marker for distinguishing serous OC from other cancer types. A well-established association between WT1 expression and an unfavorable prognosis in OC is well-documented [50,51]. Specifically, WT1 has been found to be expressed in 71.4 % of LGSOC and in 57.1 % of HGSOC [50]. The serum levels of CA125 are a valuable indicator for anticipating responses to chemotherapy, as well as for assessing the risk of relapse and disease progression in patients with OC [52]. Although it exhibits limited sensitivity in detecting stage I disease and specificity, CA125 is recognized as a predictive marker for preinvasive OC [53,54]. Elevated CA125 levels are also associated with a higher likelihood of recurrence or disease progression [55]. To compare PDTOs to their original tumors, we performed H&E staining on neoplastic tissue sections and evaluated the expression of PAX8, WT1, CA125, TP53 and Pin1 (potential) proteins as OC biomarker (Fig. 2A). Marker expression levels were evaluated and quantified as shown in Fig. 2B, revealing no statistically significant differences between primary tumor/ascites and corresponding PDTOs, indicating that PDTOs faithfully recapitulate the structural and molecular features of their tissue of origin.

Validating organoid stability in long-term cultures

All PDTOs included in this study were successfully expanded and subjected to comprehensive characterization to verify their fidelity in recapitulating the histological and molecular features

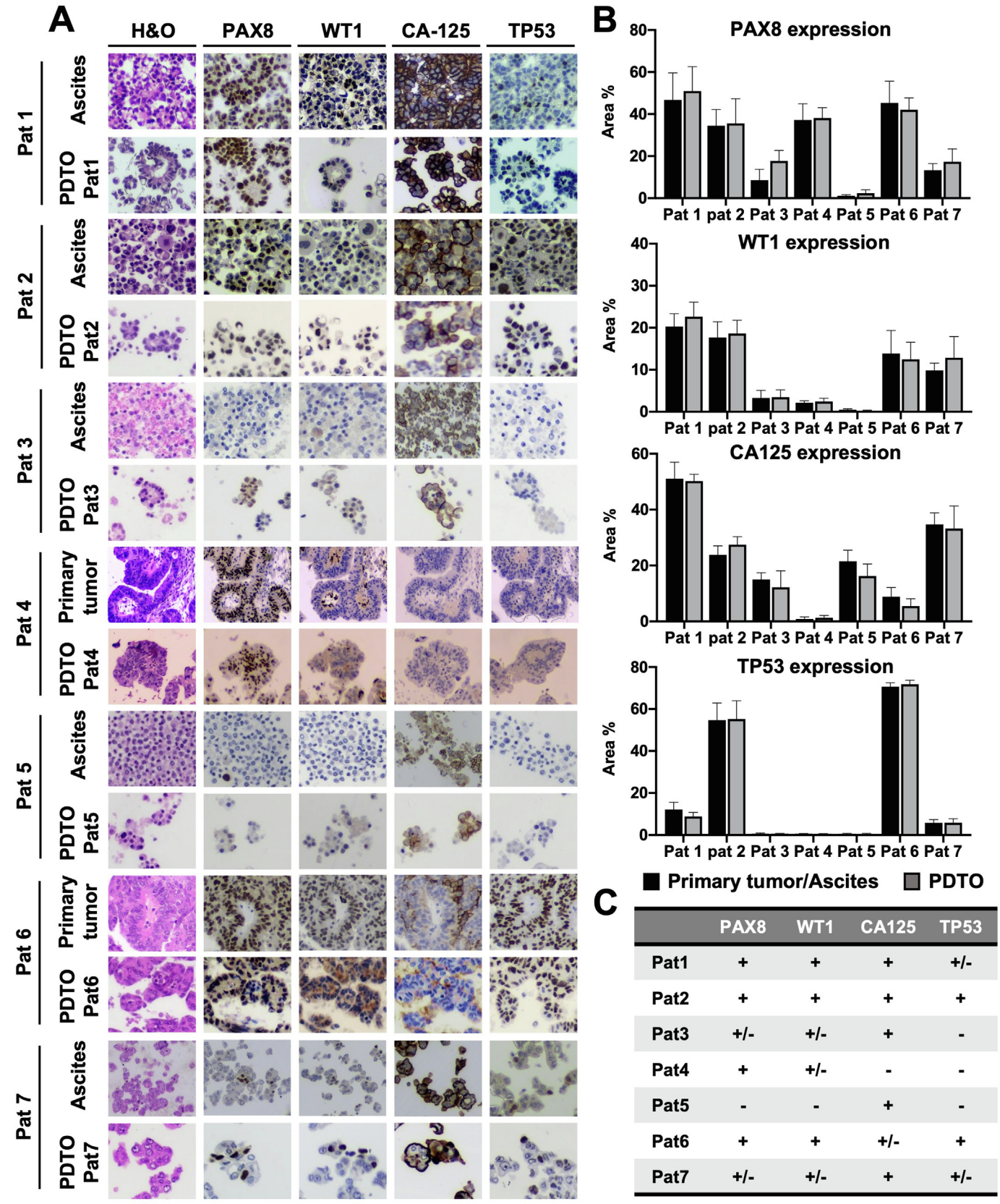

C

	PAX8	WT1	CA125	TP53
Pat1	+	+	+	+/-
Pat2	+	+	+	+
Pat3	+/-	+/-	+	-
Pat4	+	+/-	-	-
Pat5	-	-	+	-
Pat6	+	+	+/-	+
Pat7	+/-	+/-	+	+/-

Fig. 2. Organoids recapitulate the structure and characteristics at morphological and molecular levels of the tumors from which they are derived: (A) H&E staining and IHC of ascites derived from HGSOC (Patient 2, 3, 7), LGSOC (Patient 1), advanced CCC (Patient 5) and HGSOC primary tumor tissues (Patient 4, 6). CA125 (cancer antigen 125), WT1 (Wilms' Tumor 1), PAX8 (P aired box gene 8) and TP53 were done. (B) The percentage area of marker expression, as determined by IHC, was calculated in both primary tissue/ascites and PDTOs. The bar graph illustrates the mean and SD; (C) summary table of the positivity or negativity of PDTOs to the IHC markers.

of the corresponding primary tumor tissues. Following expansion, the PDTOs were cryopreserved to establish a dedicated biobank for OC models. Such biobanks are indispensable for the long-term preservation and accessibility of clinically relevant *in vitro* models, facilitating both fundamental and translational research in oncology. Biobanking protocols commonly involve multiple freeze–thaw cycles, necessitating the development of models that maintain phenotypic and functional stability over time—an essential requirement for their application in personalized therapeutic strategies.

Prior to initiating clinical correlation studies, a series of validation experiments was conducted to assess the reproducibility of PDTOs across both short- and long-term cultures. In parallel, morphology, proliferation, proteomic profiles, and drug response assays were systematically compared between early- and late-passage PDTOs, in order to ensure the consistency and reliability of treatment response data over prolonged *in vitro* culture periods.

PDTOs morphology, growth and proteomic profile

The 3D organoid structure is formed within 2–4 days of culturing and displays inter-patient morphological heterogeneity. As reported by Maenhoudt et al., the physical structure of organoids varied among samples from patients with epithelial OC, showing distinct characteristics [26,56,57].

As shown in Fig. 3A, some PDTOs exhibited a compact and dense structure with little to no central cavity (derived from Patients 2, 5, 6, and 7), while others displayed a more disorganized architecture characterized by weak intercellular cohesion, defined as low-cohesive (Patients 3 and 4). Additionally, a subset presented a cyst-like morphology (Patient 1), defined by a thin layer of cells surrounding a prominent central cavity, in line with previous findings by Kopper et al. [23]. Furthermore, viability was measured over a 9-day period, and no statistically significant differences were observed in the growth rate between low- and high-passage PDTOs (Fig. 3B). The maintenance of the structural mor-

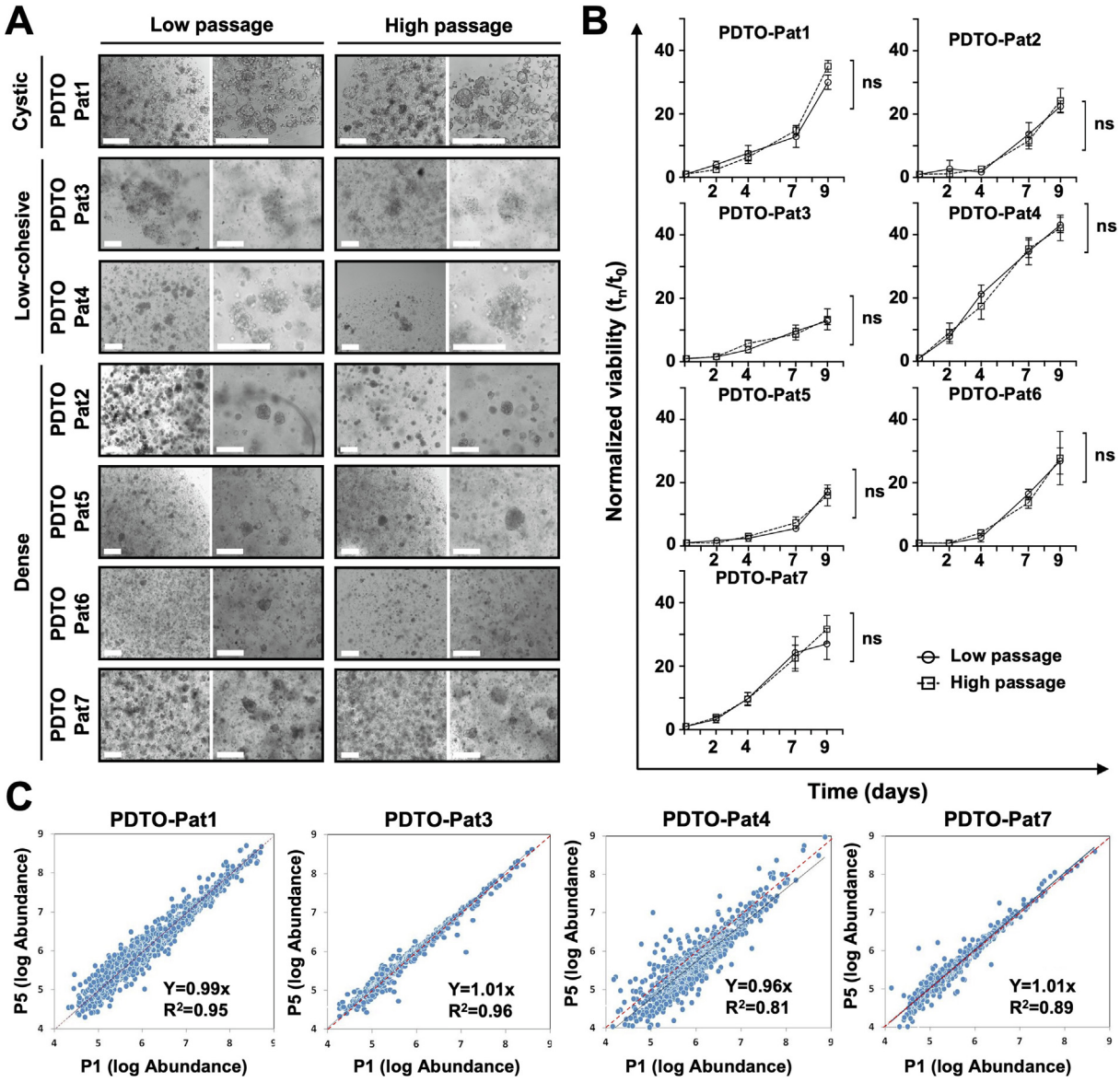

Fig. 3. Conservation of morphological and proteomic profiles in PDTOs over time: (A) Different morphology of OC organoids. Representative bright- field images of organoid cultures at low and high passages (Short and Long-term expansion). Scale bar is 200 µm. (B) Growth curve of the PDTOs. Cell viability was measured using PrestoBlue HS Assay, mean ± SD is reported; (C) Scatterplot of the protein abundance of 4 PDTOs (PDTO-Pat1, 3, 4, and 7) at low and high passages. The abundance of every protein is calculated as a triplicate and shown as a dot in the graph. The coefficient of regression was between 0.81 and 0.96, while the slope was between 0.96 and 1.01.

phology as well as the growth rate over time suggest that the phenotype remains conserved over time.

A proteomic profile of the PDTOs derived from patients 1, 3, 4, 7 was established. The abundance of the proteins at low and high passage was measured and compared.

Protein expression at low passage was found to be strongly correlated with expression at high passage (Fig. 3C); measurements at low passage were closely correlated with those measured at high passage. More than the 80 % of the analyzed proteins do not undergo significant changes indicating that the proteomic profile of PDTOs remains relatively stable over time. This result is in accordance with the experiment conducted by Kooper et al. [23] in which was evaluated the genomic landscape of copy number variations (CNV) between early and late passage HGSOC organoids [23]. Their findings revealed that CNVs were remarkably preserved even after extended passages, thereby confirming that organoids maintain a consistent protein expression profile even at later stages.

A drug screening profile in short- and long-term organoid cultures

Finally, pharmacological response of PDTOs to drugs was assessed in both short-term and long-term cultures. PDTOs were exposed to serial dilutions of selected FDA-approved drugs for 96 h, after which cell viability was assessed to generate dose–response curves. From these curves, the area under the curve (AUC) and, for effective drugs, the IC50 values were calculated. As shown in Fig. 4A, which presents an example of drug treatments on PDTOs from Patient 7, the dose–response curves exhibited no statistically significant differences between short-term and long-term PDTO cultures, regardless of drug efficacy. This observation extended to the IC_{50} and AUC values, as illustrated in Fig. 4B and C, where no statistically significant differences were observed between treatments in low- and high-passage PDTOs. This experiment was systematically repeated for all drugs and PDTO models included in the study. As depicted in Fig. 4D and E, a linear correlation was observed between IC_{50} and AUC values calculated from short- and long-term PDTO cultures. These findings are consistent with the results reported by Van de Wetering et al., who demonstrated that, for certain compounds, AUC values remained stable across different passages in colon-derived PDTOs [40].

Drug response correlation among ex-vivo PDTOs and patients

Dose–response curves were used to derive IC_{50} values (Fig. 5A), which were subsequently used to generate the heatmap, as reported in I figure supplementary 1 and Fig. 5b. This approach enabled the distinction between drug-resistant and drug-sensitive PDTOs, as well as the identification of varying degrees

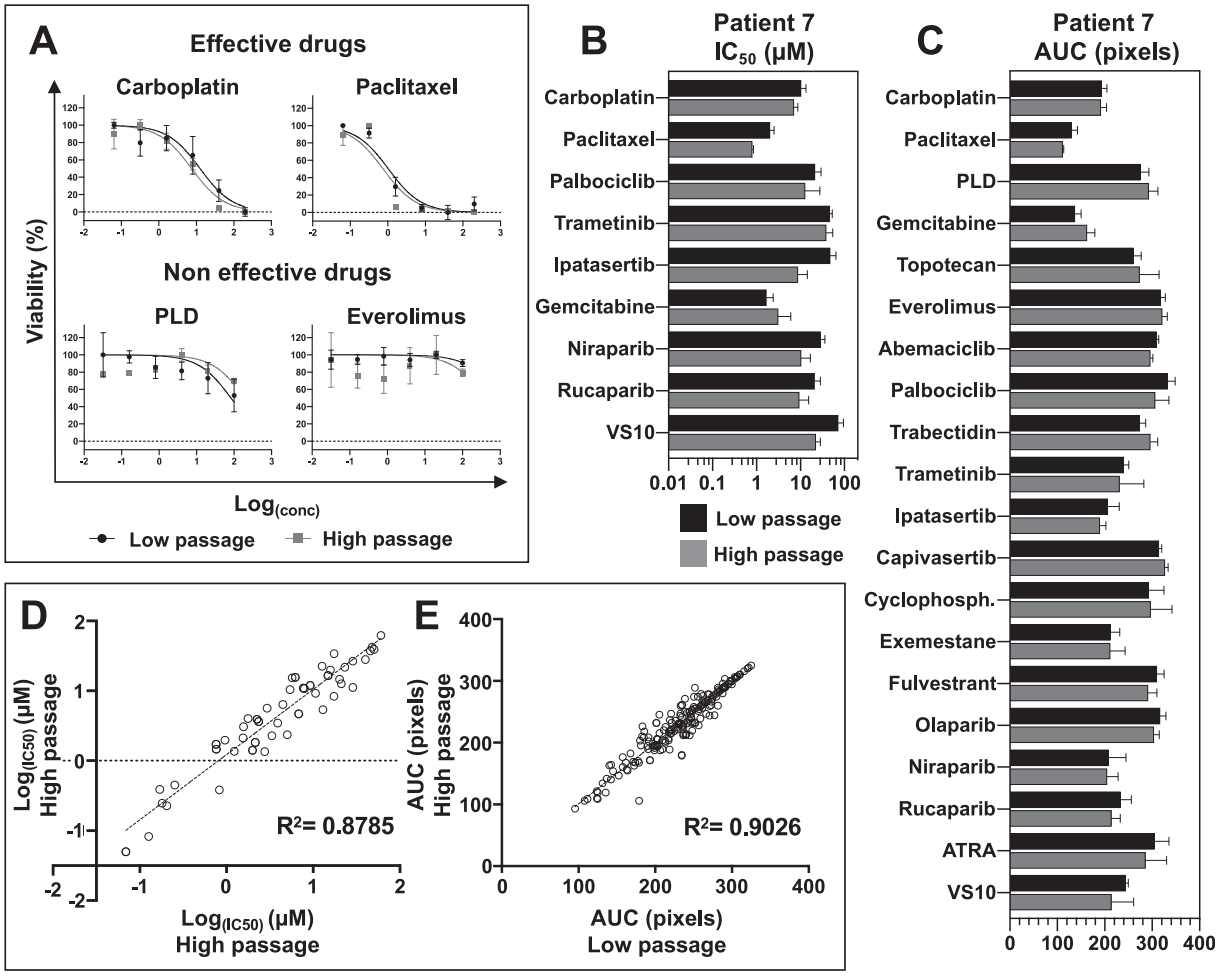

Fig. 4. PDTOs maintain the ability of predict patient response to drugs over time: (A) Comparison between high and low passage dose–response curves of the same drugs: dots represent the mean and error bars represent the SD of quintuplicates. (B) Reproducibility of drug response profiles for effective drugs in PDTO-Pat7 at low and high passages. Bars represent IC50 values from 5 replicates, with SD reported. (C) Reproducibility of drug response profiles for effective drugs in PDTO-Pat7 at low and high passages. Bars represent AUC values from 5 replicates, with SD reported. Scatterplot illustrating the correlation of $log_{(IC50)}$ values (D) and AUC (E) at low and high passages for all the PDTOs. Each point represents a replicate of 5 values. The linear correlation coefficient, calculated as the Pearson coefficient, is reported in the figure.

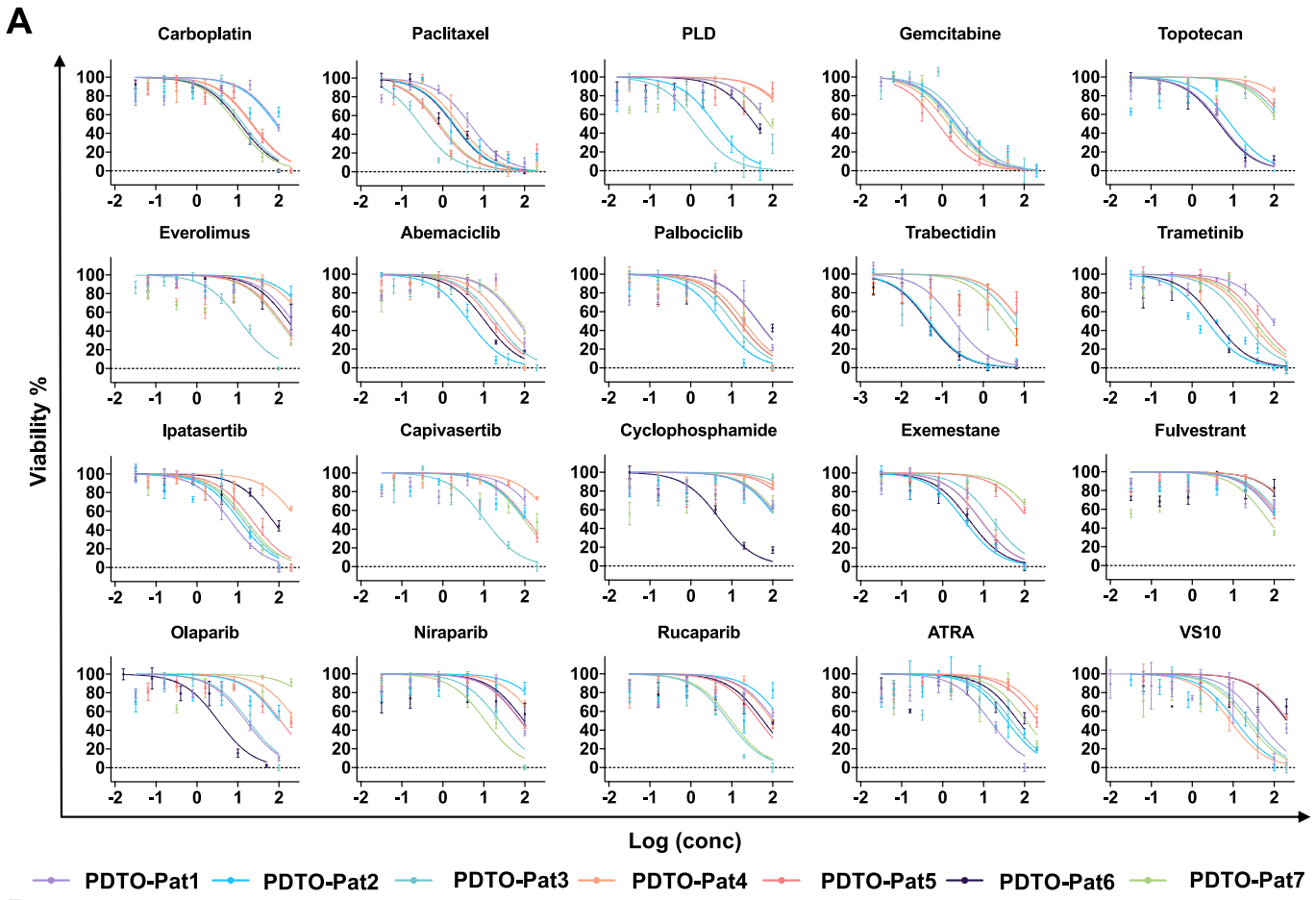

B

	Mode of action	PDTO Pat1	PDTO Pat2	PDTO Pat3	PDTO Pat4	PDTO Pat5	PDTO Pat6	PDTO Pat7
Carboplatin	DNA Crosslink							
Paclitaxel	Microtubule-stabilizing							
PLD	DNA crosslink, topoisomerase II inhibitor							
Gemcitabine	Nucleoside analog							
Topotecan	Topoisomerase I inhibitor							
Everolimus	mTOR inhibitor							
Abemaciclib	CDK4/6							
Palbociclib	CDK4/6							
Trabectidin	DNA damaging, modifies transcription							
Trametinib	MEK inhibitor							
Ipatasertib	AKT inhibitor							
Capivasertib	AKT inhibitor							
Cyclophosphamide	DNA crosslink							
Exemestane	Aromatase inhibitor, antiestrogen							
Fulvestrant	Antiestrogen							
Olaparib	PARP inhibitor							
Niraparib	PARP inhibitor							
Rucaparib	PARP inhibitor							
ATRA	PIN1 inhibitor							
VS10	PIN1 inhibitor							

Fig. 5. OC organoids as a platform for drug screening: (A) Dose–response curves of the PDTOs treated with the compounds. Dots represent the mean of the ten replicates (average of the five replicates for low and high passage each's). Error bars represent the SEM. Dose-response curves were generated with GraphPad Prism 7.0b software. (B) A heatmap derived from the IC50 values was designed for all the patients, in particular grey represent "resistance to the drug", blue/green "effective drug", red "very effective drug" and white (ND) "non determined".

of sensitivity, as illustrated in Fig. 5B (blue/green: "effective drug"; red: "highly effective drug"). The resulting *in vitro* data were then compared with the corresponding patients' clinical outcomes to establish correlations, as detailed below.

The PDTO-Pat1 was derived from ascites after palliative paracentesis for a relapsed platinum resistant LGSOC previously treated with platinum salts, taxanes, antracyclin, tamoxifen and letrozole. According to the real clinical benefit, the PDTO showed resistance

to carboplatin, Pegylated Liposomal Doxorubicin (PLD) while it was sensitive to paclitaxel (7-months clinical benefit) and gemcitabine (6-months clinical benefit). These *in vitro* sensitivities corresponded to *in vivo* responses of 6 months to weekly paclitaxel and gemcitabine (the longest PFSs experienced by the patients). Interestingly, the PDTO was resistant to trametinib, a targeted agent actually in label for this rare histotype. The patient received trametinib, but it was discontinued for adverse events (nausea and vomiting) and rapid disease progression. Trabectedin and topotecan for which the PDTO showed sensitivity, were not administered in clinic. The second patient was diagnosed with advanced HGSOC, germline BRCA1 mutated, which would typically confer sensitivity to platinum-based chemotherapy and PARP inhibitors such as olaparib. The PDTO-Pat2 was derived from ascites when she experienced a partially platinum-sensitive relapse after primary platinum-based chemotherapy and maintenance with olaparib for 6 months. According to the clinical benefit, the PDTO was resistant to carboplatin and olaparib, as for other available PARP inhibitors. This result is noteworthy given the potential utility of PDTO even in the presence of strong and clinically validated predictive biomarker as the BRCA mutation. In fact, the clinical benefit from olaparib was unusually short (6 months) even in the presence of a BRCA mutation and this was in line to the resistance to olaparib observed in the PDTO. For this reason, we explore other potential alterations in genes that could provide resistance to PARP inhibitors. We found only a TP53 splice site mutation (c.783-1G > T, VMF 0.5), likely affecting mRNA splicing and p53 function. However, no alterations associated with resistance to PARP inhibitors were identified.

The third patient showed a high spectrum of responsiveness to compounds, in particular platinum salts, taxanes and PARPi. This patient was not amenable for upfront or interval cytoreduction and was addressed for a primary platinum-based chemotherapy with a normalization of CA125 (from 100 UI/ml to 23 UI/ml). Maintenance with niraparib was started after a complete biochemical response for 6 months when the patient experiences a disease recurrence. She died few months later. To explore whether this rapid relapse could be recapitulated *in vitro*, we performed a stepwise selection experiment on PDTOs derived from this patient. Upon exposure to increasing carboplatin concentrations, the organoids progressively acquired resistance. As shown in Supplementary Fig. 2, viability assays and live/dead staining revealed the gradual emergence of drug-resistant clones, closely mirroring the rapid development of resistance observed in the patient.

The fourth patient performed the primary cytoreduction in our Institute and then was referred in a near-home hospital for medical therapy. The PDTO was obtained from the tumor tissue and no data regarding clinical response to therapies was obtained. The fifth patient was diagnosed with advanced clear cell carcinoma. After primary therapy, the patient experienced a platinum-sensitive recurrence and at that time, the PDTO was obtained from ascites. The *in vitro* sensitivity to platinum corresponded to the platinum-free interval of 12 months seen in clinic while resistance to other drugs observed *in vitro* corresponded to the known chemoresistance of this histotype. Patients 5 died for early treatment failure. She experienced disease recurrence during first line platinum therapy and she received only one cycle of non platinum therapy (liposomal doxorubicin) before death. The sixth patient was diagnosed with a mixed histology high grade serous and mucinous intestinal-like OC. She was treated with first line platinum-paclitaxel therapy and then maintenance with bevacizumab. The clinical benefit and responsiveness to platinum correspond to the platinum sensitivity of the PDTO derived from primary tumor ascites. The patient is alive and disease-free. The seventh patient was diagnosed with HGSOC at the age of 90 years. She experiences a clinical benefit from single agent carboplatin, but she had a disease progression after the 5th administration.

Notably, the *in vitro* drug response profiles observed in PDTOs demonstrated a complete concordance with the corresponding clinical outcomes, yielding a 100 % correlation. This high degree of alignment highlights the strong translational relevance of the model in the context of personalized therapy, enabling the prediction of drug resistance and the identification of alternative treatment options with the potential to improve patient survival.

Pin1 as an innovative target in OC therapy

This platform, previously validated through patient-matched clinical data for its capacity to accurately predict therapeutic responses, can also be employed as a functional tool for drug discovery. In particular, it enabled the evaluation of Pin1 inhibitors in comparison with standard-of-care agents used in OC treatment. Our research group has previously demonstrated, as reported by Russo Spena et al., that Pin1 is overexpressed in HGSOC patients and that silencing Pin1 reduces tumor cell proliferation both *in vitro* and *in vivo* [43]. This suggests that Pin1 could serve as an innovative target for OC.

IIHC analysis revealed that Pin1 expression is comparable between primary tumors and their matched PDTOs (Fig. 6A and B), with overexpression observed in 4 out of 7 PDTO models (Fig. 6B). Notably, Pin1 inhibitors demonstrated efficacy exclusively in PDTOs exhibiting Pin1 overexpression (Fig. 6C). Specifically, ATRA was effective in PDTO1 and PDTO2, while VS10 showed activity in PDTO1, PDTO2, PDTO4, and PDTO7 (Fig. 6C). These results are not surprising since, as previously reported by Russo Spena et al. [44], VS10 is a more potent Pin1 inhibitor compared to ATRA. These findings are in line with the results obtained by Cavarzerani et al. who developed a passive microfluidics platform to perform a drug screening in PDTOs of HGSOC in which 2 out of 5 PDTOs of the study were sensitive to ATRA [33]. Furthermore, in line with findings from Saorin et al. [27], Pin1 inhibitors appear to exhibit an expression-dependent effect, as they are effective only in PDTOs where Pin1 is overexpressed (PDTO1, 2, 4, and 7). Nevertheless, it should be noted that the IC_{50} values of VS10 in some models are in the high micromolar range. Given the lack of clinical pharmacokinetic data for VS10, further formulation optimization and dedicated PK/PD studies will be necessary to fully assess its translational potential.

Notably, in some cases (PDTO1 and PDTO2), Pin1 inhibitors were effective in patients resistant to Carboplatin, which is the leading therapy for OC (Fig. 5).

Conclusions

Comprehensive analyses confirm that OC PDTOs preserve the histopathological features and biomarker expression profiles of the original tumors, including markers such as PAX8, WT1, CA125, and TP53. The PDTOs and corresponding ascites/primary tumors remained highly similar at the proteomic level, even after extended passaging. This consistency is further reflected in drug response assays, where treatment sensitivity remains stable across passages. These findings are particularly critical for biobanking purposes, as PDTOs are subject to repeated freeze–thaw cycles, thereby necessitating models that demonstrate robust and sustained stability over time.

Furthermore, this PDTO model has demonstrated its capability to replicate the patient's response to therapeutic treatment in a clinical validation study. A compelling example of its potential in personalized therapy is provided by the case of PDTO-Pat2, derived from a patient harboring a germline BRCA1 mutation. PARP inhibi-

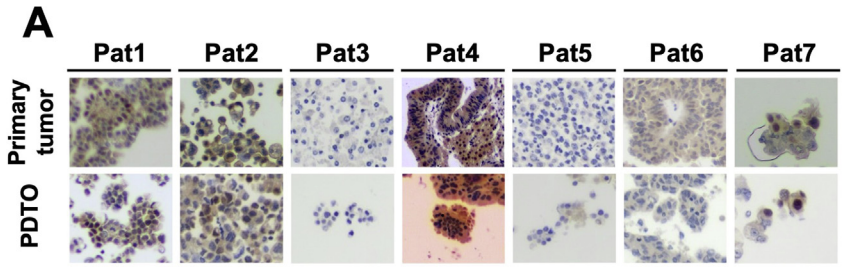

C

	IC_{50} (μM) of Pin1 inhibitors						
	PDTO Pat1	PDTO Pat2	PDTO Pat3	PDTO Pat4	PDTO Pat5	PDTO Pat6	PDTO Pat7
ATRA	6.3 ± 2.4	30.6 ± 6.8	> 100	> 200	> 200	> 200	> 200
VS10	62.5 ± 15.2	5.6 ± 1.6	> 100	6.6 ± 7.5	> 200	> 200	22.3 ± 6.2

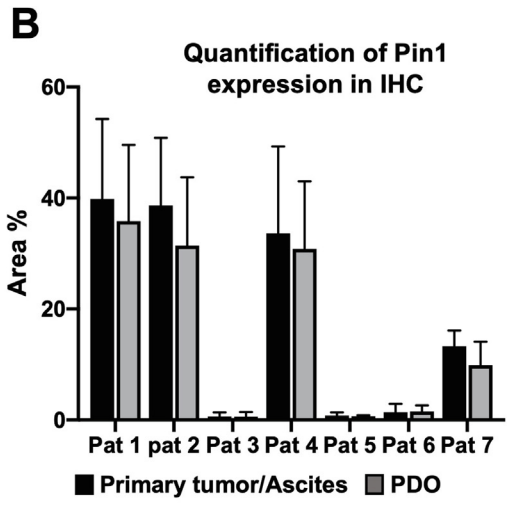

Fig. 6. Effectiveness of Pin1 Inhibitors in PDTOs with Pin1 Overexpression: (A) Immunohistochemistry of Pin1 in ascites derived from HGSOC (Patient 2, 3, 7), LGSOC (Patient 1), advanced clear cell carcinoma (Patient 5) and HGSOC primary tumor tissues (Patient 4, 6) (B) The percentage area of marker expression, as determined by IHC, was calculated in both primary tissue/ascites and PDTOs. The bar graph illustrates mean of 7 replicates, with SD; (C) IC50 values (μM) of ATRA and VS10 are reported. Data were obtained from four replicates. The numbers represent the mean and SD.

tors are standard-of-care maintenance therapy for HGSOC cancer following platinum-based treatment. However, approximately 50 % of patients experience disease recurrence and develop resistance to both platinum and PARP inhibitors—even in the presence of BRCA1/2 mutations or homologous recombination deficiency (HRD). In such cases, the use of a predictive preclinical model could offer valuable guidance to clinicians regarding treatment selection. This acquires even greater importance in diseases like OC, where in the platinum and PARP inhibitor resistance setting there are currently no validated biomarkers to guide the clinician's choice among standard single agent chemotherapy. Moreover, PDTO could serve as a platform for new drugs screening to foster the advent of new treatments in clinic.

Finally, this PDTO model has demonstrated the effectiveness of Pin1 inhibitors in a subset of OC patients where Pin1 was overexpressed. It is worth noting that in two cases, these inhibitors were even effective in patients resistant to platinum-based therapy. These data suggest that Pin1 could be a valid and innovative target for OC therapy.

Disclaimer

This manuscript has undergone grammar and syntax correction using ChatGPT, an AI language model developed by OpenAI. While every effort has been made to improve the clarity and accuracy of the language in this document, the authors acknowledge that the final content and scientific interpretations remain the sole responsibility of the authors and their collaborators. ChatGPT has been used exclusively to enhance the manuscript's readability and expression, and not to generate any type of data.

Funding acquisition

This research was funded by Fondazione AIRC per la Ricerca sul Cancro (Grant AIRC IG23566) (F.R.).

Compliance with ethics requirements

All the procedures were in accordance with the ethical standards of the committee on human experimentation (institutional and national) and with the Helsinki Declaration of 1975, as revised in 2008. This study was approved by the Ethics Committee, with approval number [17197]. Informed consent was obtained from all participants before their inclusion in the study.

Data availability

The data supporting the findings of this study are available within the paper, supplementary Information files and from the corresponding authors upon reasonable request. Source of data are provided with this paper.

Declaration of competing interest

The authors declare that they have no known competing financial interests or personal relationships that could have appeared to influence the work reported in this paper.

Appendix A. Supplementary data

Supplementary data to this article can be found online at https://doi.org/10.1016/j.jare.2025.08.009.

References

[1] Chiu WC, Ou DL, Tan CT. Mouse models for immune checkpoint blockade therapeutic research in oral cancer. Int J Mol Sci 2022;23(16):9195. doi: https://doi.org/10.3390/IJMS23169195.
[2] Chulpanova DS, Kitaeva KV, Rutland CS, Rizvanov AA, Solovyeva VV. Mouse tumor models for advanced cancer immunotherapy. Int J Mol Sci 2020;21 (11):4118. doi: https://doi.org/10.3390/IJMS21114118.
[3] Li E, Lin L, Chen CW, Ou DL. Mouse models for immunotherapy in hepatocellular carcinoma. Cancers 2019;11(11):1800. doi: https://doi.org/10.3390/CANCERS11111800.
[4] Yee C, Dickson KA, Muntasir MN, Ma Y, Marsh DJ. Three-dimensional modelling of ovarian cancer: from cell lines to organoids for discovery and personalized medicine. Front Media SA 2022. doi: https://doi.org/10.3389/fbioe.2022.836984.
[5] Colvin EK, Howell VM. Why the dual origins of high grade serous ovarian cancer matter. Nat Commun 2020;11(1):1–4. doi: https://doi.org/10.1038/s41467-020-15089-z.
[6] Perets R et al. Transformation of the fallopian tube secretory epithelium leads to high-grade serous ovarian cancer in Brca;Tp53;Pten models. Cancer Cell 2013;24(6):751–65. doi: https://doi.org/10.1016/J.CCR.2013.10.013.
[7] Kim J, Coffey DM, Creighton CJ, Yu Z, Hawkins SM, Matzuk MM. High-grade serous ovarian cancer arises from fallopian tube in a mouse model. Proc Natl

Acad Sci USA 2012;109(10):3921–6. doi: https://doi.org/10.1073/PNAS.1117135109/SUPPL_FILE/PNAS.201117135SI.PDF.
[8] Nair J et al. Resistance to the CHK1 inhibitor prexasertib involves functionally distinct CHK1 activities in BRCA wild-type ovarian cancer. Oncogene 2020;39 (33):5520–35. doi: https://doi.org/10.1038/s41388-020-1383-4.
[9] Lupia M et al. Integrated molecular profiling of patient-derived ovarian cancer models identifies clinically relevant signatures and tumor vulnerabilities. Int J Cancer 2022;151(2):240–54. doi: https://doi.org/10.1002/IJC.33983.
[10] Garziera M et al. Identification of novel somatic TP53 mutations in patients with high-grade serous ovarian cancer (HGSOC) using next-generation sequencing (NGS). Int J Mol Sci 2018;19(5):1510. doi: https://doi.org/10.3390/IJMS19051510.
[11] Javellana M et al. Neoadjuvant chemotherapy induces genomic and transcriptomic changes in ovarian cancer. Cancer Res 2021;82(1):169–76. doi: https://doi.org/10.1158/0008-5472.CAN-21-1467/674072/AM/NEOADJUVANT-CHEMOTHERAPY-INDUCES-GENOMIC-AND.
[12] Zhang S, Zhang T, Dolgalev I, Ran H, Levine DA, Neel BG, Both fallopian tube and ovarian surface epithelium can act as cell-of-origin for high grade serous ovarian carcinoma, bioRxiv 2018; 481200, doi: 10.1101/481200.
[13] Hao D et al. Integrated analysis reveals tubal- and ovarian-originated serous ovarian cancer and predicts differential therapeutic responses. Clin Cancer Res 2017;23(23):7400–11. doi: https://doi.org/10.1158/1078-0432.CCR-17-0638/14700/AM/INTEGRATED-ANALYSIS-REVEALS-TUBAL-AND-OVARIAN.
[14] JCB: Perspective How do we define organoids and 3D cultures?, 2017, doi: 10.1083/jcb.201610056.
[15] Sato T et al. Single Lgr5 stem cells build crypt-villus structures in vitro without a mesenchymal niche. Nature 2009;459(7244):262–5. doi: https://doi.org/10.1038/nature07935.
[16] Eiraku M, et al., Cell stem cell article self-organized formation of polarized cortical tissues from ESCs and its active manipulation by extrinsic signals, Stem Cell, 3:519–32, doi: 10.1016/j.stem.2008.09.002.
[17] Hill SJ et al. Prediction of DNA repair inhibitor response in short term patient-derived ovarian cancer organoids. Cancer Discov 2018;8(11):1404. doi: https://doi.org/10.1158/2159-8290.CD-18-0474.
[18] Bose S, Clevers H, Shen X. Promises and challenges of organoid-guided precision medicine. Med (N Y) 2021;2(9):1011. doi: https://doi.org/10.1016/J.MEDJ.2021.08.005.
[19] Kessler M et al. The Notch and Wnt pathways regulate stemness and differentiation in human fallopian tube organoids. Nat Commun 2015;6. doi: https://doi.org/10.1038/NCOMMS9989.
[20] Iyer S et al. Genetically DEFI ned syngeneic mouse models of ovarian cancer as tools for the discovery of combination immunotherapy. Cancer Discov 2021;11(2):384–407. doi: https://doi.org/10.1158/2159-8290.CD-20-0818/333548/AM/GENETICALLY-DEFINED-SYNGENEIC-MOUSE-MODELS-OF.
[21] Lemaçon D et al. MRE11 and EXO1 nucleases degrade reversed forks and elicit MUS81-dependent fork rescue in BRCA2-deficient cells. Nat Commun 2017;8 (1). doi: https://doi.org/10.1038/s41467-017-01180-5.
[22] Baranski Z et al. Aven-mediated checkpoint kinase control regulates proliferation and resistance to chemotherapy in conventional osteosarcoma. J Pathol 2015;236(3):348–59. doi: https://doi.org/10.1002/PATH.4528.
[23] Kopper O et al. An organoid platform for ovarian cancer captures intra- and interpatient heterogeneity. Nat Med 2019;25(5):838–49. doi: https://doi.org/10.1038/s41591-019-0422-6.
[24] Nanki Y et al. Patient-derived ovarian cancer organoids capture the genomic profiles of primary tumours applicable for drug sensitivity and resistance testing. Sci Rep 2020;10(1):1–11. doi: https://doi.org/10.1038/s41598-020-69488-9.
[25] Tao M et al. Developing patient-derived organoids to predict PARP inhibitor response and explore resistance overcoming strategies in ovarian cancer. Pharmacol Res 2022;179:106232. doi: https://doi.org/10.1016/J.PHRS.2022.106232.
[26] Maenhoudt N et al. Developing organoids from ovarian cancer as experimental and preclinical models. Stem Cell Reports 2020;14(4):717. doi: https://doi.org/10.1016/J.STEMCR.2020.03.004.
[27] Saorin G et al. Enhanced activity of a pluronic F127 formulated Pin1 inhibitor for ovarian cancer therapy. J Drug Deliv Sci Technol 2023;87. doi: https://doi.org/10.1016/j.jddst.2023.104718.
[28] Scattolin T, et al., Unlocking the potential of organopalladium complexes for high-grade serous ovarian cancer therapy, 2024, doi: 10.26434/CHEMRXIV-2024-BD942.
[29] Bortolamiol E et al. Palladium(II)-indenyl complexes bearing N-heterocyclic carbene (NHC) ligands as potent and selective metallodrugs toward high-grade serous ovarian cancer models. J Med Chem 2024;67(16):14414–31. doi: https://doi.org/10.1021/ACS.JMEDCHEM.4C01203/SUPPL_FILE/JM4C01203_SI_007.CSV.
[30] Maddaloni M et al. In vitro and in vivo evaluation of the effects of drug 2c and derivatives on ovarian cancer cells. Pharmaceutics 2024;16(5):664. doi: https://doi.org/10.3390/PHARMACEUTICS16050664/S1.
[31] Tonon G et al. Unveiling the promising anticancer activity of palladium(II)–aryl complexes bearing diphosphine ligands: a structure–activity relationship analysis. Dalton Trans 2024;53(19):8463–77. doi: https://doi.org/10.1039/D4DT00919C.
[32] Bortolamiol E et al. Rational design of palladium(II) indenyl and allyl complexes bearing phosphine and isocyanide ancillary ligands with promising antitumor activity. Molecules 2024;29(2):345. doi: https://doi.org/10.3390/MOLECULES29020345/S1.
[33] Cavarzerani E, Caligiuri I, Bartoletti M, Canzonieri V, Rizzolio F. 3D dynamic cultures of HGSOC organoids to model innovative and standard therapies. Front Bioeng Biotechnol 2023;11. doi: https://doi.org/10.3389/fbioe.2023.1135374.
[34] Scattolin T et al. Palladium(II)-η3-allyl complexes bearing N-trifluoromethyl N-heterocyclic carbenes: a new generation of anticancer agents that restrain the growth of high-grade serous ovarian cancer tumoroids. Chem Eur J 2020;26(51):11868–76. doi: https://doi.org/10.1002/CHEM.202002199.
[35] Tzouras NV et al. A green synthesis of carbene-metal-amides (CMAs) and carboline-derived CMAs with potent in vitro and ex vivo anticancer activity. ChemMedChem 2022;17(13):e202200135. doi: https://doi.org/10.1002/CMDC.202200135.
[36] Scattolin T et al. The anticancer activity of an air-stable Pd(I)-NHC (NHC = N-heterocyclic carbene) dimer. Chem Commun 2020;56(81):12238–41. doi: https://doi.org/10.1039/D0CC03883K.
[37] Saorin A, et al., Microfluidic production of amiodarone loaded nanoparticles and application in drug repositioning in ovarian cancer, 123AD, doi: 10.1038/s41598-024-55801-3.
[38] Granchi C et al. Design, synthesis and biological evaluation of second-generation benzoylpiperidine derivatives as reversible monoacylglycerol lipase (MAGL) inhibitors. Eur J Med Chem 2021;209:112857. doi: https://doi.org/10.1016/J.EJMECH.2020.112857.
[39] Wensink GE et al. Patient-derived organoids as a predictive biomarker for treatment response in cancer patients. NPJ Precis Oncol 2021;5. doi: https://doi.org/10.1038/S41698-021-00168-1.
[40] Van De Wetering M et al. Prospective derivation of a living organoid biobank of colorectal cancer patients. Cell 2015;161(4):933–45. doi: https://doi.org/10.1016/j.cell.2015.03.053.
[41] Senkowski W et al. A platform for efficient establishment and drug-response profiling of high-grade serous ovarian cancer organoids. Dev Cell 2023;58 (12):1106–1121.e7. doi: https://doi.org/10.1016/j.devcel.2023.04.012.
[42] Jabs J et al. Screening drug effects in patient-derived cancer cells links organoid responses to genome alterations. Mol Syst Biol 2017;13(11). doi: https://doi.org/10.15252/msb.20177697.
[43] Russo Spena C et al. Liposomal delivery of a Pin1 inhibitor complexed with cyclodextrins as new therapy for high-grade serous ovarian cancer. J Control Release 2018;281:1–10. doi: https://doi.org/10.1016/J.JCONREL.2018.04.055.
[44] Russo Spena C et al. Virtual screening identifies a PIN1 inhibitor with possible antiovarian cancer effects. J Cell Physiol 2019;234(9):15708–16. doi: https://doi.org/10.1002/jcp.28224.
[45] Brooks EA, Galarza S, Gencoglu MF, Chase Cornelison R, Munson JM, Peyton SR. Applicability of drug response metrics for cancer studies using biomaterials. Royal Society Publishing; 2019. doi: 10.1098/rstb.2018.0226.
[46] Ford CE, Werner B, Hacker NF, Warton K. The untapped potential of ascites in ovarian cancer research and treatment. Br J Cancer 2020;123(1):9–16. doi: https://doi.org/10.1038/s41416-020-0875-x.
[47] Hardy LR, Salvi A, Burdette JE. UnPAXing the divergent roles of PAX2 and PAX8 in high-grade serous ovarian cancer. Cancers 2018;10(8):262. doi: https://doi.org/10.3390/CANCERS10080262.
[48] Nik SA et al. Upregulation of Wilms' tumor gene 1 (WT1) in desmoid tumors. Int J Cancer 2005;114(2):202–8. doi: https://doi.org/10.1002/IJC.20717.
[49] Koesters R et al. WT1 is a tumor-associated antigen in colon cancer that can be recognized by in vitro stimulated cytotoxic T cells. Int J Cancer 2004;109 (3):385–92. doi: https://doi.org/10.1002/IJC.11721.
[50] Sallum LF et al. WT1, p53 and p16 expression in the diagnosis of low- and high-grade serous ovarian carcinomas and their relation to prognosis. Oncotarget 2018;9(22):15818–27. doi: https://doi.org/10.18632/ONCOTARGET.24530.
[51] Netinatsunthorn W, Hanprasertpong J, Dechsukhum C, Leetanaporn R, Geater A. WT1 gene expression as a prognostic marker in advanced serous epithelial ovarian carcinoma: an immunohistochemical study. BMC Cancer 2006;6 (1):1–9. doi: https://doi.org/10.1186/1471-2407-6-90/FIGURES/3.
[52] Gupta D, Lis CG. Role of CA125 in predicting ovarian cancer survival – A review of the epidemiological literature. J Ovarian Res 2009;2(1):1–20. doi: https://doi.org/10.1186/1757-2215-2-13/TABLES/9.
[53] van der Burg MEL, Lammes FB, Verweij J. CA125 in ovarian cancer. Neth J Med 2007;40(1–2):36–51. doi: https://doi.org/10.2217/17520363.1.4.513.
[54] Duffy M et al. CA125 in ovarian cancer: European Group on Tumor Markers guidelines for clinical use. Int J Gynecol Cancer 2004. doi: https://doi.org/10.1136/IJGC-00009577-200509000-00001.
[55] Charkhchi P, Cybulski C, Gronwald J, Wong FO, Narod SA, Akbari MR. CA125 and ovarian cancer: a comprehensive review. Cancers 2020;12(12):3730. doi: https://doi.org/10.3390/CANCERS12123730.
[56] Maenhoudt N, Vankelecom H. Protocol for establishing organoids from human ovarian cancer biopsies. STAR Protoc 2021;2(2):100429. doi: https://doi.org/10.1016/J.XPRO.2021.100429.
[57] Maenhoudt N, et al., Stem cell reports article developing organoids from ovarian cancer as experimental and preclinical models, doi: 10.1016/j.stemcr.2020.03.004.